Prediction of histological grade using preoperative multi-sequence MRI-based radiomics signature in patients with non-small-cell lung cancer

Xing Tang

  Department of Radiology, Xijing Hospital, Fourth Military Medical University, Xi'an, Shaanxi

Guoyan Bai

  Department of Clinical Laboratory , Shaanxi Provincial People's Hospital, Xi'an, Shaanxi

Yuanqiang Zhu

  Department of Radiology, Xijing Hospital, Fourth Military Medical University, Xi'an, Shaanxi

Hong Wang

  Department of Radiology, Xijing Hospital, Fourth Military Medical University, Xi'an, Shaanxi

Jian Zhang

  Department of Respiratory Medicine, Xijing Hospital, Fourth Military Medical University, Xi'an, Shaanxi

Fan Guo

  Department of Radiology, Xijing Hospital, Fourth Military Medical University, Xi'an, Shaanxi

Hong Yin (✉ yinnhong@163.com)

  Department of Radiology, Xijing Hospital, Fourth Military Medical University, Xi'an, Shaanxi

---

Research Article

Abstract

Background: Non-small cell lung cancer (NSCLC) is treatable when caught early, yet limited non-invasive methods exist for grading NSCLC patients. In the present study, we aimed to examine the diagnostic utility of multi-sequence magnetic resonance imaging (MRI) radiomics and clinical features for grading NSCLC.

Methods: In this retrospective study, 148 patients with postoperative pathologically-confirmed NSCLC were recruited. Both preoperative T2-weighted imaging (T2WI) and multi-b-value diffusion-weighted imaging (DWI) were performed on a 1.5 T MRI scanner. A total of 2775 radiomics features were extracted from the T2WI, DWI, and the corresponding apparent diffusion coefficient (ADC) maps of patients. The least absolute shrinkage and selection operator (LASSO) and stepwise regression method were used for feature selection using the training cohort (n=110). Next, these features were further evaluated assessed in the two cohorts using a non-linear support vector machine (SVM) classifier. Lastly, a *Radscore* model was used to develop the radiomics-clinical nomogram.

Results: Favorable discrimination performance was obtained for five of the optimal features using both cohorts, as demonstrated by the area under the curves (AUC) of 0.761 and 0.753. In addition, the radiomics-clinical nomogram, which integrated the *Radscore* with four independent clinical predictors, showed higher discriminative power, with AUCs of 0.814 and 0.767 for the X.T cohort and H.Y cohort, respectively. The nomogram showed excellent predictive performance and potential clinical utility for grading NSCLC.

Conclusions: Multi-sequence MRI radiomics features can stratify NSCLC tumor grades noninvasively. The radiomics features can be integrated with the clinical features to improve its predictive performance.

Background

Although there have been rapid developments for diagnosing and treating lung cancer in recent years [1,2], lung cancer accounts for approximately 13% of all cancer-related cases each year. In addition, it remains the highest cause of cancer-related mortality worldwide [3]. Non-small-cell lung cancer (NSCLC) is the most common form of lung cancer, accounting for up to 85% of the primary lung malignancies diagnosed each year, with a 5-year survival rate of less than 20% [4]. Histopathological differentiation plays an essential role in the prognosis and behavior of lung cancer [5]. For example, poorly differentiated, high-grade lung cancer has a poorer prognosis and an elevated risk of lymph node metastasis, local recurrence, and death than well-differentiated, low-grade tumors [6]. Tumor grading has implications beyond predicting the prognosis of patients with lung cancer, and also affect the treatment plan [7].

Biopsies remain the gold standard for determining the tumor grade. While computed tomography (CT)-guided percutaneous lung biopsy and endobronchial biopsy are common techniques used in clinical practice. However, these biopsy techniques have limitations, as they fail to reflect the overall tumor

condition owing to the small size of the extraction site [8, 9]. Moreover, biopsies are highly invasive and can cause physical and psychological trauma to patients, in addition to the risk of complications during surgery [10]. For these reasons, a non-invasive method for preoperatively predicting NSCLC tumor histology grades is desired. Currently, medical imaging is an essential tool for diagnosing NSCLC, as studies have reported strong positive correlations between specific imaging markers and tumor grades. For example, dynamic multiphase net enhancement and multidetector CT (MDCT) perfusion parameters can help grade the differentiation of tumors [11, 12]. In addition, apparent diffusion coefficient (ADC) values in diffusion-weighted imaging (DWI) sequences of magnetic resonance (MR) can distinguish between high-grade and low-grade lung cancers. In other words, the ADC values of high-grade lung cancer are significantly lower than those of low-grade lung cancer [13, 14]. As another example, the standard uptake value (SUV) of positron emission tomography (PET) is higher for high-grade lung cancer due to vascular stroma and fibrosis [11]. However, the use of perfusion CT is limited in patients with increased radiation doses [15], and DWI overlaps in the ADC values of high- and low-grade lung cancer [13]. Additionally, PET is more expensive than other imaging methods. Hence, newer non-invasive imaging techniques are needed to provide improved information for accurately grading tumors in the clinic.

In recent years, breakthroughs have been made in the acquisition, standardization, and analysis of medical images, which have improved made it possible to turn the accurate and quantitative image descriptions into non-invasive biomarkers for predicting the prognosis of cancer [16]. Radiomics is an emerging field based on advanced pattern recognition. Using radiomics, researchers can extract quantitative features from digital images to determine the relationship between the features and the pathophysiology of tissues [17, 18]. Currently, the radiomics strategies have been based on multi-sequence magnetic resonance imaging (MRI) data, including T2-weighted images (T2WI) and DWI. The respective ADC images have been used for discriminating various cancers, including renal carcinoma, bladder cancer, prostate cancer, and soft tissue sarcoma, making it possible to accurately assess the histological grades and predict outcomes [19-22]. However, it remains unknown if multi-sequence MRI-extracted radiomics features can accurately reflect differences between histological grades of tumors.

Hence, in this study, we investigated the feasibility of a multi-sequence MRI radiomics strategy for grading NSCLC. Secondly, we developed and validated a radiomics-clinical nomogram model for individualized risk stratification of NSCLC patients using a combination of imaging radiomics features and clinical factors.

Methods

The retrospective study was approved by the institutional ethics review board of Xijing Hospital (Xi'an, China). Due to the retrospective design, the requirement for informed consent was waived by the committee. All methods were performed in accordance with the relevant guidelines and regulations. Additional information about the study design is shown in **Fig. 1**.

Patients

Between January 2015 and December 2018, patients confirmed with squamous cell carcinomas or adenocarcinomas of the lung postoperatively were included from a single clinical center. The inclusion criteria were (1) MRI examination within two months of surgical pathology results or biopsy pathology results; (2) no other history of malignant tumors; and (3) lesions were larger than 8 mm to ensure adequate count statistics and consistent analysis of the region of interest (ROI). The exclusion criteria were (1) lung cancer had been treated prior to MRI, such as chemotherapy or radiotherapy; (2) no pathological results obtained after MRI; (3) MRI showed artifacts or the data could not be measured or analyzed; and (4) patients had contraindications to MRI (e.g., cochlear implants and pacemakers). (5) Only the largest tumor was used in cases of multifocal or multicentric lung cancer. In total, 148 patients (112 males and 36 females; mean age, 59 ± 11 years; age range, 20-79 years) were included in this study. The age and gender of patients were obtained from the medical records, while tumor characteristics, including the histological type and degree of tumor differentiation, were obtained from the pathological records.

Histological grades were assessed by two pathologists independently, both more than nine years of clinical experience. The resected tumors were classified into grade 1 or well-differentiated (n = 11), grade 2 or moderately differentiated (n = 60), and grade 3 or poorly differentiated (n = 77). Due to the small number of grade 1 tumors, the patients were divided into two groups for the analysis, including a low-grade group containing well-differentiated and moderately-differentiated tumors and a high-grade group containing poorly-differentiated tumors. Among the groups, 110 patients (84 males and 26 females) were randomly selected as the training model for development, and 38 (28 males and ten females) were used for performance verification. For this study, clinical features consisted of sex, age, smoking status, side of lung involvement, location of tumor, and histology subtypes (CEA, Ki-67, LPD, LD). These characteristics were obtained from archived medical records.

MR image acquisition and ROI delineation

MR examinations were performed using the MAGNETOM Aera 1.5 T scanner from Siemens Medical Solutions (Erlangen, Germany). The scanner had an eight-channel phased-array torso coil. T2-weighted and diffusion-weighted MRI sequences were used in this study. A bi-exponential model (b = 50 or 800 sec/mm^2) was used to obtain the ADC maps automatically. For more information about the sequence parameters, please visit the Supplementary Materials.

Prior to delineating the ROI, an axial image slice from each MRI system was obtained by identifying the largest tumor area with the maximum size in the lung region of each patient. The tumor area on the selected image was selected using a manually drawn polygonal ROI. Since the DWI was used to calculate the ADC map with a double exponential model, the ROIs were placed onto the ADC maps to determine the respective tumor regions. Tumors were manually drawn by two radiologists independently (with nine and five years of MRI diagnostic experience in lung cancer) using the custom-developed package ITK-SNAP

software (www.itksnap.org). When the ROI selection diverged, the differences were negotiated and corrected to select a consistent ROI. Details about the delineation of ROIs are shown in **Fig. 1**.

Extraction of imaging features

High-dimensional radiological features were extracted from the ROI of the tumor using the MRI data to describe the tumor phenotype. The features were divided into four groups: (1) 13 graphic intensity features, (2) seven shape size features, (3) 165 high-order texture (RLM, NGTDM, and GLSZM) features, and (4) 740 wavelet features. Every single image contained 925 features, with 2775 features in three images, which fully described the local and regional tissue distributional changes in the tumor. For example, the first group described the gray histogram of the tumor region and the voxel's gray distribution. The second group primarily described the tumor phenotype, including the shape, area, volume, and compactness of the circles and burrs. The third group showed the uniformity or heterogeneity of the tumor's internal structure. The fourth group showed the intensity and texture of the image by decomposing the original image. All of the features have been utilized in previous radiomics studies [16, 23]. Because the original T2WI, DWI, and ADC images were of different gray levels prior to the high-order GLRLM, NGTDM, and GLSZM texture feature extraction, all tumor ROIs described for the three MRI sequences adopted a multi-grade normalization strategy. In other words, all tumor ROI gradations of the three MRIs were normalized (each feature, minus the mean divided by the standard deviation, converted to a mean of 0, with a standard deviation of 1). We used a publicly shared MATLAB software package, and the features were extracted online [24, 25].

Selection of features, evaluation of predictive performance, and generation of Radscore

A combination of methods has been assessed for their discriminatory abilities in low- and high-grade NSCLC [26]. First, features were selected using the Student's t-test, and 42 features that were significantly different between the two grades in the training cohort were identified. A logistic regression analysis was performed using the least absolute shrinkage and selection operator (LASSO) regularization to determine which features showed the best predictive value for histological classification. LASSO is a shrinkage and variable selection strategy for the regression of high-dimensional data [27]. As LASSO requires tuning of the model parameter (λ), ten-fold cross-validation was used for tuning parameter (λ) selection in the LASSO model. After the LASSO regression, a total of 17 features remained. Next, for the combination case, the 17 features were further reduced using the stepwise regression, of which five features were finally selected. The performance of the tool was evaluated using the two cohorts. All of these processes were achieved using the cv.glmnet function from the glmnet package under the platform R v. 3.2.3. In the next step, a logistic regression algorithm was applied using the five optimal features in the training group, which made it possible to obtain the coefficient of each feature, along with the intercept for generating the *Radscore* formula [24, 25]. Using the formula, the *Radscores* for the patients were calculated for further studies.

Development of the radiomics-clinical nomogram and assessment of its predictive performance

The clinical usefulness of the radiomics model for discriminating between low- and high-grade NSCLC was evaluated using methods already described in the literature [26]. Briefly, the univariate and multivariate regression analyses were performed using the *Radscore* and clinical features from the training cohort. Next, the nomogram was created using the independent predictors from the training cohort. The predictive performance of the nomogram was quantitatively evaluated the training and validation cohorts for its sensitivity, specificity, accuracy, and area under the curve (AUC) of the receiver operating characteristic (ROC) [24, 25]. The Hosmer-Lemeshow tests, used to determine the agreement between the expected and actual observations, and the decision curve analyses, were conducted to determine the precision and potential clinical utility of the model.

Statistical analysis

Statistical analysis was conducted using the R statistical software (version 3.4.4, x64). *P*-values of < 0.05 were considered significant. Both univariate and multivariate regression analyses were used to identify independent predictors for the discrimination task.

Results

Patient characteristics

The baseline demographics and clinical data of patients from the training and validation cohorts are shown in **Table 1**. The characteristics of patients in the training and validation cohorts were not significantly different.

Performance of the optimal features selected to discriminate the histological grade

After assessing 2775 radiomics features from the training cohort, 42 features were found to be significantly different between the two histological grades. Next, the LASSO method was applied to the salient features, and 17 were selected. Forward-backward stepwise regression was used to select five major features as the optimal features, and a logistic regression model was constructed (**Figures 2A and 2B**).

Calculation of Radscore

To further simplify the prediction model, the logistic regression algorithm was used to generate the *Radscore* formula based on the best features. **Figure 2B** showed the coefficients of each feature. The formula's intercept was -0.555. **Figure 2C** showed the sum of the absolute coefficients of these features on the image class, from which the features of the DWI image contributed the most to calculating the *Radscore*. Using this formula to calculate the *Radscore* and ROC curves for the two patient cohorts (**Figures 3A and 3B**) yielded a significant difference ($p < 0.01$) between the low- and high-grade NSCLC cases (**Figure 3C**).

The radiomics-clinical nomogram's performance in thediscrimination of high- and low-grade NSCLC

To enhance its recognition performance, univariate and multivariate analyses were performed in conjunction with clinical factors and *Radscore*. The combination of *Radscore* with clinical factors revealed that sex, smoking, and *Radscore* were independent predictors of recognition tasks (**Table 2**).

In the next step, sex, smoking, and *Radscore* were integrated to obtain a nomogram model of the clinical angiographic factors (**Figure 4A**). Each patient's risk of being diagnosed with high-grade NSCLC was quantified using the nomogram model. **Figure 4B** showed that the low- and high-grade histology risk profiles differed significantly between the two cohorts ($p < 0.01$). Through our model, the recognition performance was improved greatly (**Figure 4C and Table 3**). The prediction accuracy and AUC of the training queue increased to 77.3% and 0.814, respectively, while the prediction accuracy and AUC of the verification queue increased to 78.9% and 0.767, respectively.

In addition, the *p*-value of the Hosmer-Lemeshow test was 0.893, which was not statistically significant, indicating that the prediction results of the nomogram model agreed well with the observations. Clinical effectiveness was assessed with the decision curve analysis. If the risk was higher than 0.2, the net benefit was greater than the imaging ensemble model-alone (**Figure 5**).

Discussion

In the present study, we demonstrated the construction of and validation of a radiomics-clinical nomogram based on preoperative MRI and clinical characteristics for predicting low- and high-grade NSCLC. Using the training and validation cohorts, our nomogram showed excellent discriminative power and clinical utility. Hence, our proposed nomogram may be an effective and non-invasive tool for preoperative histological grade assessment in patients with lung cancer.

Currently, there is no histological grading system with clearly defined criteria and clinical significance widely accepted for patients with lung cancer. The World Health Organization (WHO) (4th edition) classification method for lung cancer grades adenocarcinoma as 1 (good differentiation, predominantly with wall growth), 2 (moderate differentiation, with acinar or nipple), or 3 (poor differentiation, mainly solid or micropapillary) [28]. These structural patterns are based on the most important tissue classifications for adenocarcinoma. Previously, Weichert *et al.* developed a grading system for lung squamous cell carcinoma, which summarized the scores of two independent prognostic markers, including tumor sprouting and tumor nest size [29]. However, both definitions depend on the subjective judgment of the pathologist, and the hierarchy is easily confused. To study the unity of the standard, traditional histological grading methods were also used in this study, including the similarity of structural patterns to the normal lung tissue of its origin, as well as the tumor cell atypia and degree of differentiation. The traditional histology grading system has been established for many years and is clinically relevant and reproducible in breast cancer [30], prostate cancer [31], endometrial cancer [32], soft tissue sarcoma [33], and renal cancer [34]. Therefore, we assume that the traditional histological grading system is applicable in NSCLC.

From the hypothesis described above, the feasibility and performance of histological grading identification in NSCLC patients remain unclear for multi-sequence MRI ensembles. Therefore, we aimed to (1) explore and study imaging grouping strategies based on multi-sequence MRI, such as T2WI, DWI, and ADC, to preoperatively identify high- and low-grade NSCLC, and (2) verify whether the combination of radiomics features and clinical features may improve the discriminating ability of this study.

Our findings demonstrate that the radiomics features extracted from the T2WI, DWI, and ADC were strongly correlated with the histological grade of NSCLC. The double MRI sequences used in the current study are standard and used in hospitals worldwide. The radiomics-based classification of NSCLC allowed for the non-invasive prediction and stratification of high- and low-grade NSCLC. In our experiments, *Radscore* was the most effective method of distinguishing the histological grade of NSCLC. The *Radscore* combined five optimal characteristics as one biological marker. Recent studies have combined multiple marker analyses into a single individual marker [35, 36]. For example, a recent study screened 21 independent genes from patients with breast cancer. The characteristics of these 21 genes together were identified and validated as the optimal features that can prevent certain breast cancer patient groups from requiring chemotherapy [36].

The highest sum of the absolute value coefficients was obtained from the DWI features; thus, higher DWI signals showed higher tumor levels, which exhibited faster cell proliferation, higher cell densities, larger cell nuclei, higher intracellular macromolecular protein content, higher cytoplasmic ratios, smaller extracellular space [13, 37], and more limited intracellular and extracellular diffusion. As of now, DWI is the only imaging method that can detect limited cell diffusion. DWI was first used in the central nervous system, but applying this technology to the lungs is challenging due to its drawbacks, including its low signal-to-noise ratio due to the inherent low density of protons located in the lungs, image artifacts caused by the movement of the heart and the breath, and high-gradient fields that influence the magnetic susceptibility of the inflated lung tissue, which increases the likelihood of artifacts [38, 39]. Our experimental team used the ISHIM-EPI sequence to reduce magnetic-sensitive and respiratory motion artifacts. Under free-breathing conditions, the signal-to-noise ratio and image quality were improved for the DWI.

Only a few studies have explored the preoperative differentiation of NSCLC histological grades based on dual-energy CT and ADC in recent years. These tests have limitations, including CT ionizing radiation problems and overlap of ADC values [13]; however, traditional medical imaging methods have always been qualitative. The rise of imaging radiomics, the rapid development of image acquisition methods, standardization strategies, and image analysis tools have enabled researchers to objectively, accurately, and quantitatively describing tumor imaging as a non-invasive biological marker for predicting the prognosis of patients. No previous studies achieved a quantitative risk stratification of the histological level of NSCLC patients based on a nomogram model. Previously, Chen *et al.* performed image analytics based on enhanced CT to extract 591 radiomics features [40]. The minimum redundancy, maximum correlation algorithm, and logistic regression model were used to reduce dimensionality and select the best features. Finally, a model was established from nine features. A set of radiomics features was

validated in an independent validation group. The feature set was used to distinguish between high and low-grade lung cancer in the training group, of which the AUC was 0.763, and the accuracy rate was 68.7%. For comparison, the AUC was 0.782, and the accuracy rate was 71.2% in the verification group. This result was similar to our *Radscore* results from multisequence MRI radiomics. We also applied the nomogram model proposed by the clinical factor. The results were slightly better than those of the enhanced CT-based imaging radiomics method in terms of identification tasks.

Clinical features, such as age, sex, smoking, tumor location, tumor typing, longest tumor diameter, vertical tumor diameter, CEA, Ki67, and histological subtype, are commonly used to diagnose patients with lung cancer. If the combination of the factors and the feature-generated *Radscore* can improve recognition performance requires further study. Surprisingly, the univariate analysis revealed that none of these factors correlated with the grading of lung cancer. Univariate correlation is not reported to show sufficient predictive strength [41], which is a common strategy for excluding the variable from model development. However, among these predictors, nuances in the dataset may result in the exclusion of important predictors. These results may also have been due to confusion with other predictors. We also believed that all factors should be related; thus, the multifactor analysis showed that sex, smoking, and *Radscore* together were significant predictors of recognition tasks. Then, we generated the nomogram model from these predictive factors and obtained a satisfactory recognition rate with better recognition performance than that of the imaging ensemble model. Therefore, the combination of radiomics features and clinical factors can enhance its recognition ability. In addition, we also verified that the nomogram model showed good prediction accuracy and clinical application value.

This study had some limitations. First, because the study was retrospective, and the patient population was relatively limited, inherent bias may exist. The addition of more patients in a multi-center trial would help validate our findings. In addition, owing to incomplete archival database data, this study excluded other potential clinical features, including genetic mutations and possible molecular markers, which require further analysis. Third, although we used multivariate logistic regression models, ROC curves combined with nomograms as well as calibration curves, which are commonly accepted in the field of medical imaging analysis, along with other comparative studies are needed.

Conclusions

Multi-sequence MRI radiomics features could predict the histological grading of patients with NSCLC noninvasively. Additionally, the integration of radiomics features and clinical features resulted in improved performance. Hence, radiomics signatures may be a promising tool for determining the grade and treatment planning for NSCLC.

Declarations

Ethics approval and consent to participants

This study was approved by the Ethics Committee of Xijing Hospital with number KY20141104-2. Due to the retrospective design, the requirement for informed consent was waived by the committee. All methods were performed in accordance with the relevant guidelines and regulations.

Consent for publication

Not applicable.

Availability of data and materials

Competing interests

Funding

Author's contributions

XT, GYB, YQZ, JZ, FG and HY contributed to the study concept, design, and data interpretation. XT、GYB and JZ contributed to the clinical data collection. HW and XT contributed to the imaging data collection. XT, YQZ contributed to the model construction and data analysis. XT contributed to the manuscript drafting. XT, HY and FG contributed to the manuscript revision. All authors approve the final version of the manuscript. XT contributed to the manuscript submission.

Acknowledgements

References

1. Minguet J, Smith KH and Bramlage P. Targeted therapies for treatment of non-small cell lung cancer–Recent advances and future perspectives. *Int J Cancer* 2016; 138: 2549-2561. 2015/11/06. DOI: 10.1002/ijc.29915.

2. Levy B, Hu ZI, Cordova KN, et al. Clinical Utility of Liquid Diagnostic Platforms in Non-Small Cell Lung Cancer. *Oncologist* 2016; 21: 1121-1130. 2016/07/09. DOI: 10.1634/theoncologist.2016-0082.

3. Torre LA, Bray F, Siegel RL, et al. Global cancer statistics, 2012. *CA Cancer J Clin* 2015; 65: 87-108. 2015/02/06. DOI: 10.3322/caac.21262.

4. Torre LA, Siegel RL and Jemal A. Lung Cancer Statistics. *Adv Exp Med Biol* 2016; 893: 1-19. 2015/12/17. DOI: 10.1007/978-3-319-24223-1_1.

5. White NM, Cabanski CR, Silva-Fisher JM, et al. Transcriptome sequencing reveals altered long intergenic non-coding RNAs in lung cancer. *Genome Biol* 2014; 15: 429. 2014/08/15. DOI: 10.1186/s13059-014-0429-8.

6. Sun Z, Aubry MC, Deschamps C, et al. Histologic grade is an independent prognostic factor for survival in non-small cell lung cancer: an analysis of 5018 hospital- and 712 population-based cases. *J Thorac Cardiovasc Surg* 2006; 131: 1014-1020. 2006/05/09. DOI: 10.1016/j.jtcvs.2005.12.057.

7. Riely GJ and Travis WD. Can IASLC/ATS/ERS subtype help predict response to chemotherapy in small biopsies of advanced lung adenocarcinoma? *Eur Respir J* 2014; 43: 1240-1242. 2014/05/03. DOI: 10.1183/09031936.00048814.

8. Zhu X, Dong D, Chen Z, et al. Radiomic signature as a diagnostic factor for histologic subtype classification of non-small cell lung cancer. *Eur Radiol* 2018; 28: 2772-2778. 2018/02/17. DOI: 10.1007/s00330-017-5221-1.

9. Su R, Zhang J, Liu X, et al. Identification of expression signatures for non-small-cell lung carcinoma subtype classification. *Bioinformatics* 2020; 36: 339-346. 2019/07/13. DOI: 10.1093/bioinformatics/btz557.

10. Herbst RS, Heymach JV and Lippman SM. Lung cancer. *N Engl J Med* 2008; 359: 1367-1380. 2008/09/26. DOI: 10.1056/NEJMra0802714.

11. Cappabianca S, Porto A, Petrillo M, et al. Preliminary study on the correlation between grading and histology of solitary pulmonary nodules and contrast enhancement and [18F]fluorodeoxyglucose standardised uptake value after evaluation by dynamic multiphase CT and PET/CT. *J Clin Pathol* 2011; 64: 114-119. 2010/12/21. DOI: 10.1136/jcp.2010.076562.

12. Xiong Z, Liu JK, Hu CP, et al. Role of immature microvessels in assessing the relationship between CT perfusion characteristics and differentiation grade in lung cancer. *Arch Med Res* 2010; 41: 611-617. 2011/01/05. DOI: 10.1016/j.arcmed.2010.11.005.

13. Liu H, Liu Y, Yu T, et al. Evaluation of apparent diffusion coefficient associated with pathological grade of lung carcinoma, before therapy. *J Magn Reson Imaging* 2015; 42: 595-601. 2014/12/30. DOI: 10.1002/jmri.24823.

14. Tsuchiya N, Doai M, Usuda K, et al. Non-small cell lung cancer: Whole-lesion histogram analysis of the apparent diffusion coefficient for assessment of tumor grade, lymphovascular invasion and pleural invasion. *PLoS One* 2017; 12: e0172433. 2017/02/17. DOI: 10.1371/journal.pone.0172433.

15. Lin LY, Zhang Y, Suo ST, et al. Correlation between dual-energy spectral CT imaging parameters and pathological grades of non-small cell lung cancer. *Clin Radiol* 2018; 73: 412 e411-412 e417. 2017/12/10. DOI: 10.1016/j.crad.2017.11.004.

16. Aerts HJ, Velazquez ER, Leijenaar RT, et al. Decoding tumour phenotype by noninvasive imaging using a quantitative radiomics approach. *Nat Commun* 2014; 5: 4006. 2014/06/04. DOI: 10.1038/ncomms5006.

17. Kumar V, Gu Y, Basu S, et al. Radiomics: the process and the challenges. *Magn Reson Imaging* 2012; 30: 1234-1248. 2012/08/18. DOI: 10.1016/j.mri.2012.06.010.

18. Lambin P, Rios-Velazquez E, Leijenaar R, et al. Radiomics: extracting more information from medical images using advanced feature analysis. *Eur J Cancer* 2012; 48: 441-446. 2012/01/20. DOI: 10.1016/j.ejca.2011.11.036.

19. Goyal A, Razik A, Kandasamy D, et al. Role of MR texture analysis in histological subtyping and grading of renal cell carcinoma: a preliminary study. *Abdom Radiol (NY)* 2019; 44: 3336-3349. 2019/07/14. DOI: 10.1007/s00261-019-02122-z.

20. Penzias G, Singanamalli A, Elliott R, et al. Identifying the morphologic basis for radiomic features in distinguishing different Gleason grades of prostate cancer on MRI: Preliminary findings. *PLoS One* 2018; 13: e0200730. 2018/09/01. DOI: 10.1371/journal.pone.0200730.

21. Wang Y, Hu D, Yu H, et al. Comparison of the Diagnostic Value of Monoexponential, Biexponential, and Stretched Exponential Diffusion-weighted MRI in Differentiating Tumor Stage and Histological Grade of Bladder Cancer. *Acad Radiol* 2019; 26: 239-246. 2018/05/14. DOI: 10.1016/j.acra.2018.04.016.

22. Zhang Y, Zhu Y, Shi X, et al. Soft Tissue Sarcomas: Preoperative Predictive Histopathological Grading Based on Radiomics of MRI. *Acad Radiol* 2019; 26: 1262-1268. 2018/11/01. DOI: 10.1016/j.acra.2018.09.025.

23. Itakura H, Achrol AS, Mitchell LA, et al. Magnetic resonance image features identify glioblastoma phenotypic subtypes with distinct molecular pathway activities. *Sci Transl Med* 2015; 7: 303ra138. 2015/09/04. DOI: 10.1126/scitranslmed.aaa7582.

24. Xu X, Wang H, Du P, et al. A predictive nomogram for individualized recurrence stratification of bladder cancer using multiparametric MRI and clinical risk factors. *J Magn Reson Imaging* 2019; 50: 1893-1904. 2019/04/14. DOI: 10.1002/jmri.26749.

25. Xu X, Zhang X, Tian Q, et al. Quantitative Identification of Nonmuscle-Invasive and Muscle-Invasive Bladder Carcinomas: A Multiparametric MRI Radiomics Analysis. *J Magn Reson Imaging* 2019; 49: 1489-1498. 2018/09/27. DOI: 10.1002/jmri.26327.

26. Tang X, Xu X, Han Z, et al. Elaboration of a multimodal MRI-based radiomics signature for the preoperative prediction of the histological subtype in patients with non-small-cell lung cancer. *Biomed Eng Online* 2020; 19: 5. 2020/01/23. DOI: 10.1186/s12938-019-0744-0.

27. Liu Z, Zhang XY, Shi YJ, et al. Radiomics Analysis for Evaluation of Pathological Complete Response to Neoadjuvant Chemoradiotherapy in Locally Advanced Rectal Cancer. *Clin Cancer Res* 2017; 23: 7253-7262. 2017/09/25. DOI: 10.1158/1078-0432.CCR-17-1038.

28. Travis WD, Brambilla E, Nicholson AG, et al. The 2015 World Health Organization Classification of Lung Tumors: Impact of Genetic, Clinical and Radiologic Advances Since the 2004 Classification. *J*

Thorac Oncol 2015; 10: 1243-1260. 2015/08/21. DOI: 10.1097/JTO.0000000000000630.

29. Weichert W, Kossakowski C, Harms A, et al. Proposal of a prognostically relevant grading scheme for pulmonary squamous cell carcinoma. *Eur Respir J* 2016; 47: 938-946. 2015/11/07. DOI: 10.1183/13993003.00937-2015.

30. Rakha EA, Reis-Filho JS, Baehner F, et al. Breast cancer prognostic classification in the molecular era: the role of histological grade. *Breast Cancer Res* 2010; 12: 207. 2010/09/02. DOI: 10.1186/bcr2607.

31. Amin MB, Lin DW, Gore JL, et al. The critical role of the pathologist in determining eligibility for active surveillance as a management option in patients with prostate cancer: consensus statement with recommendations supported by the College of American Pathologists, International Society of Urological Pathology, Association of Directors of Anatomic and Surgical Pathology, the New Zealand Society of Pathologists, and the Prostate Cancer Foundation. *Arch Pathol Lab Med* 2014; 138: 1387-1405. 2014/08/06. DOI: 10.5858/arpa.2014-0219-SA.

32. Zaino RJ. FIGO staging of endometrial adenocarcinoma: a critical review and proposal. *Int J Gynecol Pathol* 2009; 28: 1-9. 2008/12/03. DOI: 10.1097/PGP.0b013e3181846c6d.

33. Guillou L, Coindre JM, Bonichon F, et al. Comparative study of the National Cancer Institute and French Federation of Cancer Centers Sarcoma Group grading systems in a population of 410 adult patients with soft tissue sarcoma. *J Clin Oncol* 1997; 15: 350-362. 1997/01/01. DOI: 10.1200/JCO.1997.15.1.350.

34. Cornejo KM, Dong F, Zhou AG, et al. Papillary renal cell carcinoma: correlation of tumor grade and histologic characteristics with clinical outcome. *Hum Pathol* 2015; 46: 1411-1417. 2015/08/25. DOI: 10.1016/j.humpath.2015.07.001.

35. Birkhahn M, Mitra AP and Cote RJ. Molecular markers for bladder cancer: the road to a multimarker approach. *Expert Rev Anticancer Ther* 2007; 7: 1717-1727. 2007/12/08. DOI: 10.1586/14737140.7.12.1717.

36. Sparano JA, Gray RJ, Makower DF, et al. Prospective Validation of a 21-Gene Expression Assay in Breast Cancer. *N Engl J Med* 2015; 373: 2005-2014. 2015/09/29. DOI: 10.1056/NEJMoa1510764.

37. Henzler T, Schmid-Bindert G, Schoenberg SO, et al. Diffusion and perfusion MRI of the lung and mediastinum. *Eur J Radiol* 2010; 76: 329-336. 2010/07/16. DOI: 10.1016/j.ejrad.2010.05.005.

38. Razek AA. Diffusion magnetic resonance imaging of chest tumors. *Cancer Imaging* 2012; 12: 452-463. 2012/10/31. DOI: 10.1102/1470-7330.2012.0041.

39. Bonekamp S, Corona-Villalobos CP and Kamel IR. Oncologic applications of diffusion-weighted MRI in the body. *J Magn Reson Imaging* 2012; 35: 257-279. 2012/01/25. DOI: 10.1002/jmri.22786.

40. Chen X, Fang M, Dong D, et al. A Radiomics Signature in Preoperative Predicting Degree of Tumor Differentiation in Patients with Non-small Cell Lung Cancer. *Acad Radiol* 2018; 25: 1548-1555. 2018/03/25. DOI: 10.1016/j.acra.2018.02.019.

41. Collins GS, Reitsma JB, Altman DG, et al. Transparent Reporting of a Multivariable Prediction Model for Individual Prognosis or Diagnosis (TRIPOD): The TRIPOD Statement. *Eur Urol* 2015; 67: 1142-1151. 2015/01/13. DOI: 10.1016/j.eururo.2014.11.025.

Tables

Table 1 Baseline demographics of the patients involved in this research

Characteristics	Training cohort (n=110)	Validation cohort (n=38)	p-value
Age, years			0.721
Median [range]	60 [20⬚76]	60.5 [33⬚83]	
Sex, no. (%)			0.959
Male	84/110 ⬚76.4%⬚	28/38 ⬚73.7%⬚	
Female	26/110 ⬚23.6%⬚	10/38 ⬚26.3%⬚	
Smoking, no. (%)			0.684
Yes	77/110 ⬚70%⬚	25/38 ⬚65.8%⬚	
No	33/110 ⬚30%⬚	13/38 ⬚34.2%⬚	
Side, no. (%)			0.16
Upper left lobe	29/110 ⬚26.4%⬚	16/38 ⬚42.1%⬚	
Lower left lobe	18/110 ⬚16.4%⬚	5/38 ⬚13.2%⬚	
Upper right lobe	28/110 ⬚25.5%⬚	6/38 ⬚15.8%⬚	
Middle right lobe	6/110 ⬚5.5%⬚	0/38 ⬚0%⬚	
Lower right lobe	29/110 ⬚26.4%⬚	11/38 ⬚28.9%⬚	
Location, no. (%)			0.381
Peripheral	63/110 ⬚57.3%⬚	25/38 ⬚65.8%⬚	
Centra	47/110 ⬚42.7%⬚	13/38 ⬚34.2%⬚	
LD, mm*			0.381
Median [range]	48.5 [13⬚115]	55.5 [10⬚100]	
LPD, mm*			0.484
Median [range]	35 [10⬚90]	38 [8⬚77]	
CEA⬚⬚ng/ml⬚*			0.549
Median [range]	4.7 [0.486⬚ 1135]	4.22 [0.486⬚479.2]	
Ki67⬚⬚%⬚			0.923

Median [range]	0.6 [0.07⎯3.0]	0.5 [0.1⎯0.95]	
Histological subtype, no. (%)			0.880
Squamous cell carcinoma	50/110 ⎯45%⎯	18/38 ⎯47%⎯	
Adenocarcinoma	60/110 ⎯55%⎯	20/38 ⎯53%⎯	
Histological grade⎯⎯%⎯			0.968
Low-grade	57/110 ⎯51.8%⎯	20/38 ⎯52.6%⎯	
High- and	53/110 ⎯48.2%⎯	18/38 ⎯47.4%⎯	

* LD, LPD and CEA indicate the longest diameter, the longest perpendicular diameter, and carcinoembryonic antigen, respectively

Table 2 Univariate and multivariable regression analyses of the Radscore with primary clinical features for the histological grade prediction of NSCLC

Indicators	Univariate analysis				Multivariable analysis			
	OR	95% CI		*p*-value	OR	95% CI		*p*-value
		Lower	Upper			Lower	Upper	
Age	1.678	0.683	4.121	0.259	<u>0.133</u>	<u>0.027</u>	<u>0.657</u>	<u>< 0.05</u>
Sex	0.969	0.932	1.007	0.111				
Smoking	1.210	0.535	2.738	0.647	<u>0.206</u>	<u>0.048</u>	<u>0.891</u>	<u>< 0.05</u>
Side	0.840	0.642	1.099	0.203	—	—	—	—
Location	0.949	0.445	2.020	0.891	—	—	—	—
LD*	1.021	0.855	1.218	0.818	—	—	—	—
LPD*	1.058	0.835	1.339	0.641	—	—	—	—
CEA*	0.999	0.998	1.001	0.459	—	—	—	—
Ki67	2.109	0.603	7.378	0.243	—	—	—	—
Histological subtype	0.545	0.255	1.167	0.118	—	—	—	—
Radscore	<u>2.718</u>	<u>1.661</u>	<u>4.448</u>	<u><< 0.01</u>	2.967	1.772	4.968	<u><< 0.01</u>

The underlined values indicate statistical significance with p value < 0.05 after the univariate analysis.

The italics underlined values indicate statistical significance with p value < 0.05 after the multivariable analysis.

* LD, LPD, CEA and OR indicate the longest diameter, the longest perpendicular diameter, carcinoembryonic antigen, and odds ratio, respectively.

Table 3 Performance of the radiomics-clinical nomogram in discriminating between high- and low-grade NSCLC in the training and validation cohorts

Cohort	*Sen	*Spe	*Acc	AUC	95% CI		*p*-value
					Lower	Upper	
Training	64.2%	89.5%	77.3%	0.814	0.733	0.894	< 0.01
Validation	7.8%	80.0%	78.9%	0.767	0.608	0.925	< 0.05

*Sen, Spe, Acc and AUC indicate the sensitivity, specificity, accuracy and area under the curve of the receiver operating characteristic curve, respectively

Figures
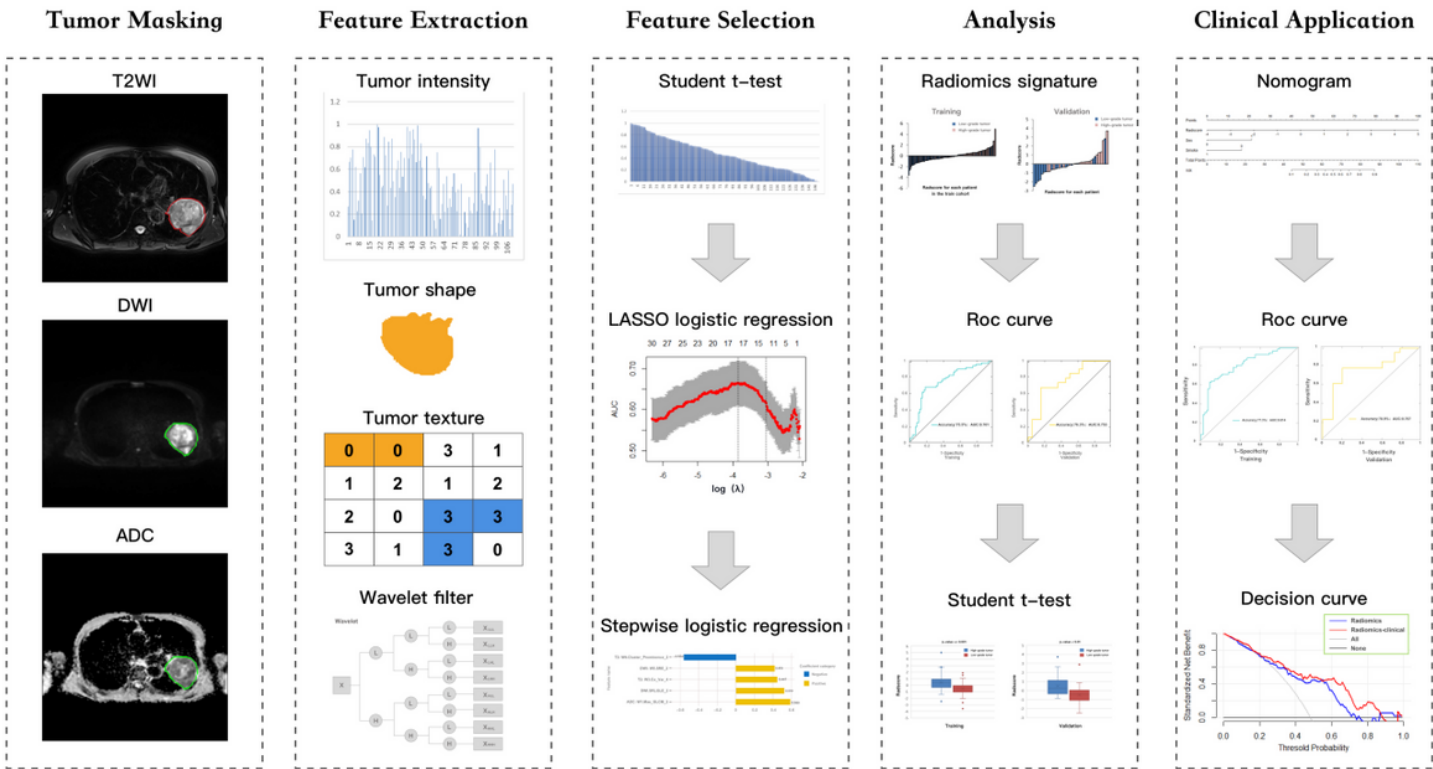
Figure 1

Schematic diagram describes the preoperative determination of high- and low-grade NSCLC.
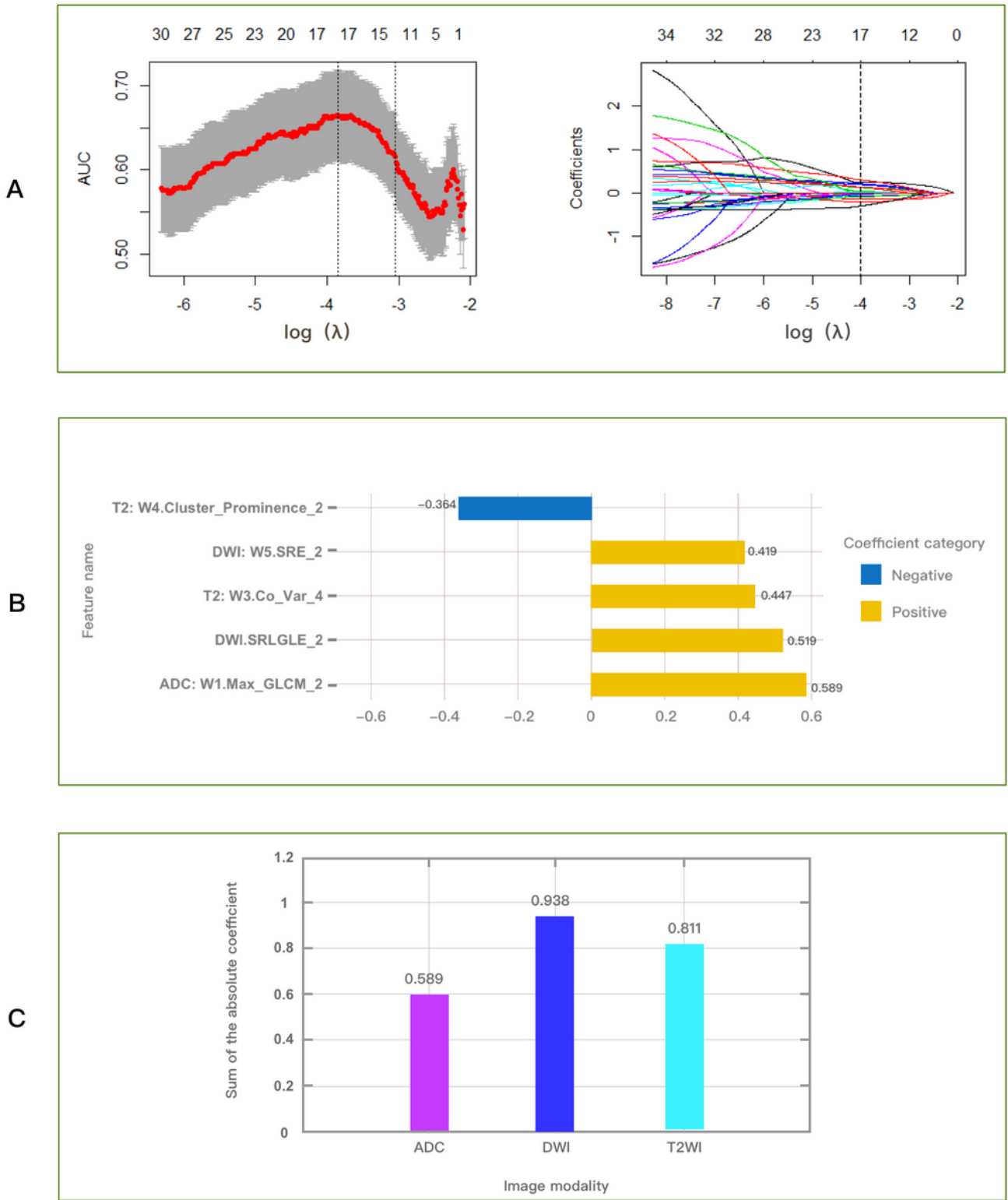

Figure 2

Selection of optimal features and the classification performance of these selected features in two groups. (A) Features selection using LASSO in the training cohort; (B) coefficient maps of five optimal features; (C) absolute value coefficients were added of the best features from the different MRI sequences, and the sum is shown.
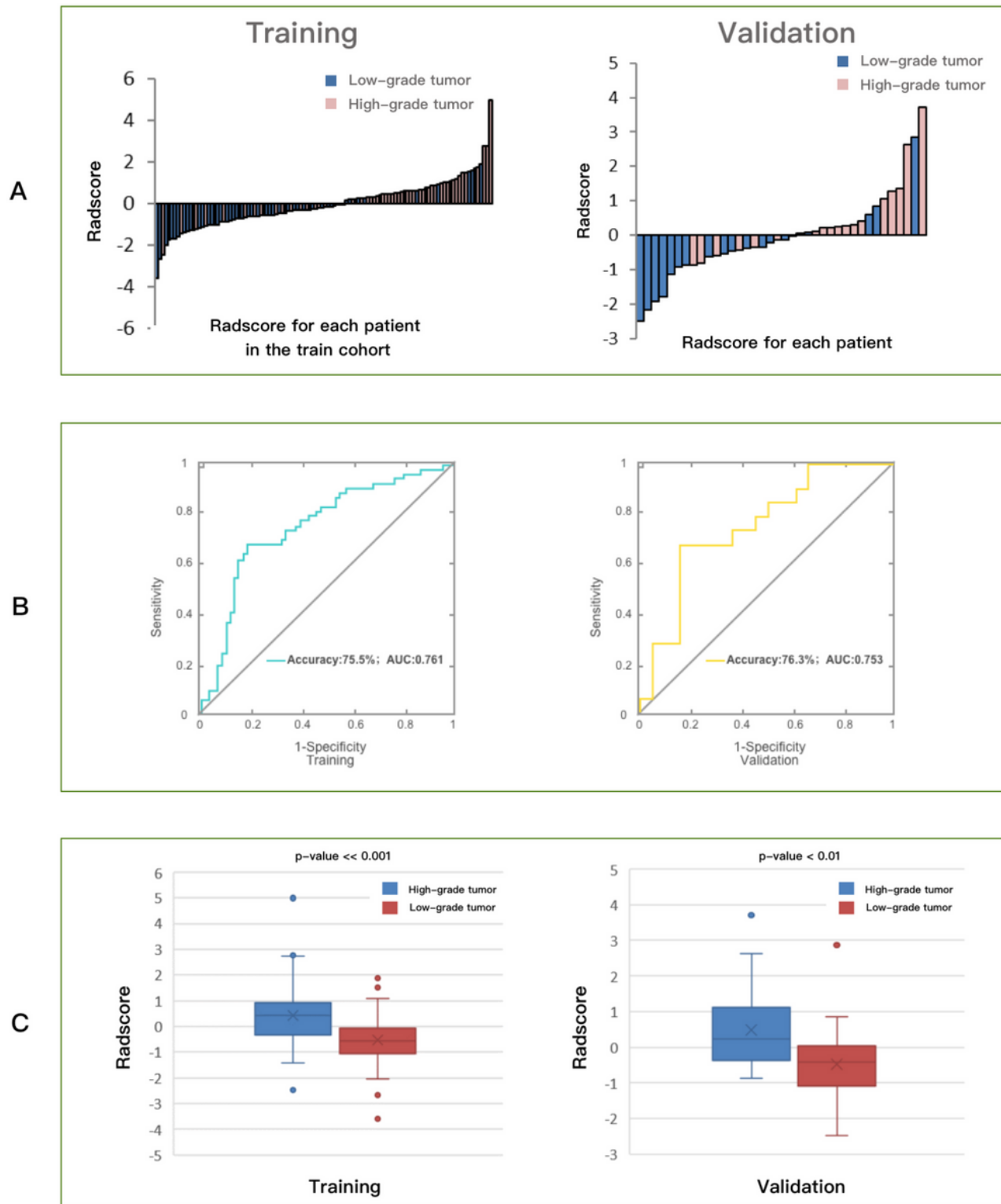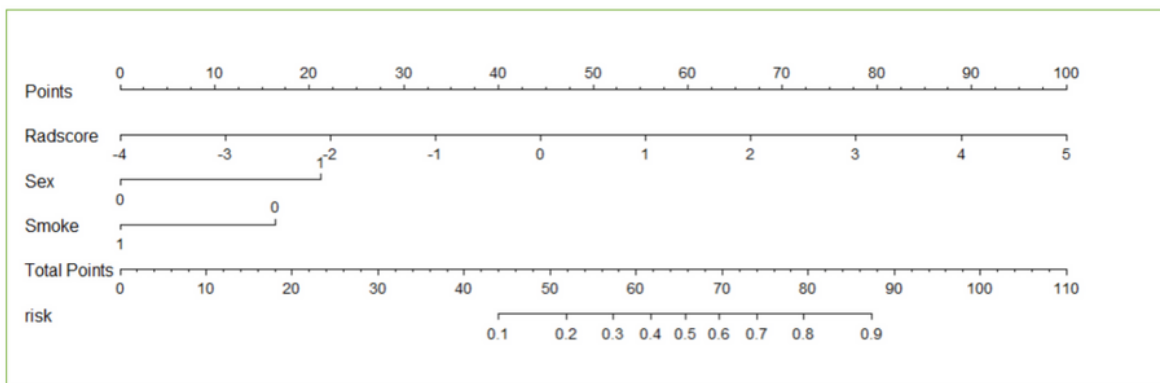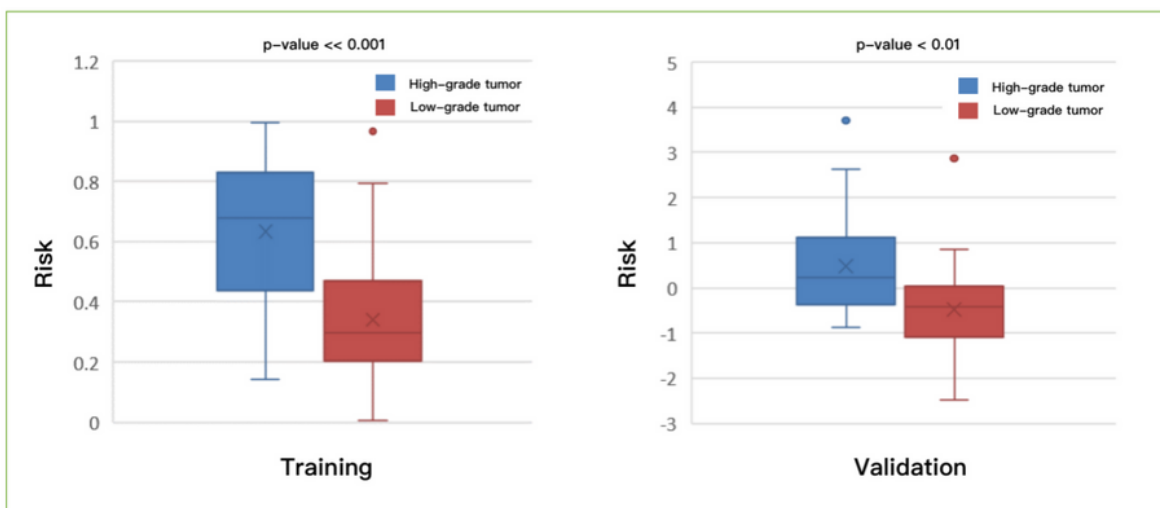
Figure 3

Radscore generation and its inter-group distribution. (A) The Radscore of each patient in training and validation cohorts; (B) selected feature performance in both cohort; (C) distribution and inter-group analyses.
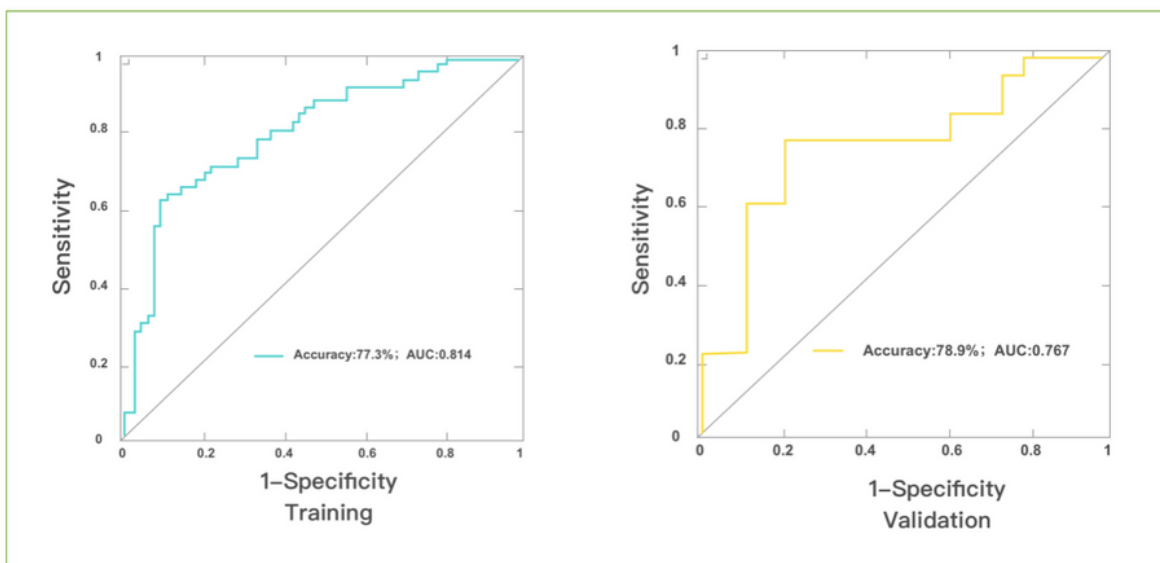
Figure 4

Development and validation of the nomogram. (A) Radscore and separate clinical indicators were used to create the nomogram; (B) calculation of risk calculated and differences in the statistical intergroup distribution; (C) verification of the nomogram's performance.
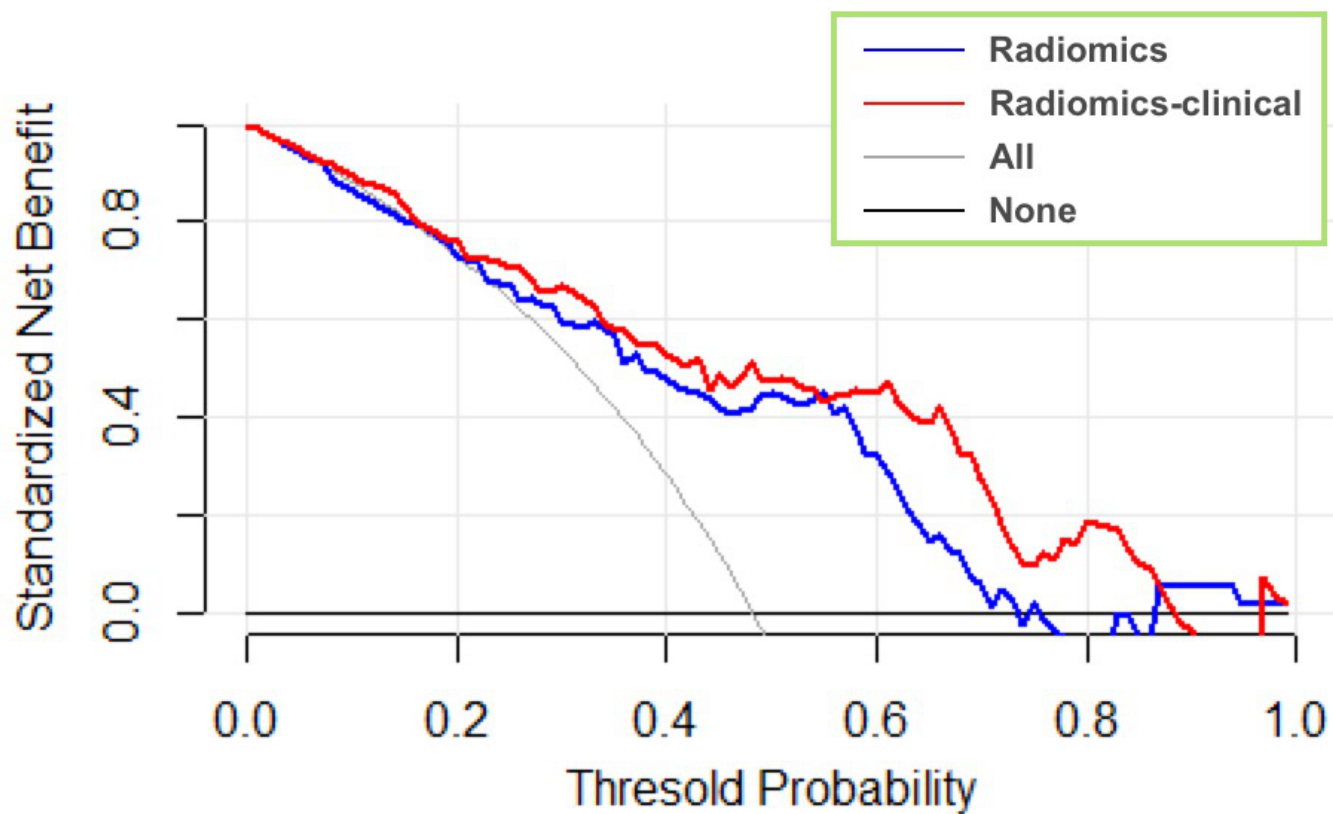
Figure 5

Clinical utility of the model, from results of the decision curve analysis, showed greater benefit from the radiomics-clinical nomogram vs. the clinical or radiomics models-alone.

Supplementary Files

This is a list of supplementary files associated with this preprint. Click to download.

- SupplementaryMaterials.docx